Supporting Information for (34 pp):

Shallow Gas Migration along Hydrocarbon Wells – An Unconsidered,

Anthropogenic Source of Biogenic Methane in the North Sea

Lisa Vielstädte,[*,†,‡] *Matthias Haeckel,*[*,†] *Jens Karstens,*[†] *Peter Linke,*[†] *Mark Schmidt,*[†] *Lea*

Steinle,[†,§] *and Klaus Wallmann*[†]

[†] *GEOMAR Helmholtz Centre for Ocean Research Kiel, 24148 Kiel, Germany*

[‡] *Department of Earth System Science, Stanford University, Stanford, California 94305, United States*

[§]*Department of Environmental Sciences, University of Basel, 4001 Basel, Switzerland*

[*]*Corresponding authors:*

L. Vielstädte *(*Phone: +1-650-305-5154; E-mail: lvielsta@stanford.edu); M. Haeckel (Phone: +49-431-600-2123; E-mail: mhaeckel@geomar.de).

Content

1. Definitions and nomenclature

Leakage: In this paper leakage is defined as "fugitive", or unintended emission of shallow gas. It is sourced from gas accumulations in the overburden of the deep hydrocarbon reservoir (i.e. in the upper 1000 m of sediment), through which the well has been drilled. To the best of our knowledge, leakage of shallow gas can be induced by any type of well (production, injection, dry, or abandoned).

Well integrity: There is no common global definition of well integrity, but the NORSOK D-010[3] definition is widely used for the North Sea. It defines well integrity as an application of technical, operational and organizational solution to reduce the risk of uncontrolled release of formation fluids throughout the life cycle of the well. Based on this definition, operators and governmental agencies perform well integrity surveys, targeting the leakage of formation fluids through the cement, casing and completion equipment, having a focus mostly on active wells, as monitoring is not mandatory after well abandonment[3].

Well: According to the Norwegian Petroleum Directorate (NPD) guidelines for designation of wells and wellbores[45], a well is defined as a borehole which is drilled in order to discover or delimit a petroleum deposit and/ or to produce petroleum or water for injection purposes, to inject gas, water or other media, or to map or monitor well parameters[45]. A well may consist of one or several wellbores (well paths) and may have one or several termination points[45].

Wellbore (well path): A wellbore/well-path designates the location of the well from one termination point to the wellhead and may consist of one or more well tracks[45].

Well track: The well track is the part of a wellbore (well path) which extends from a point of drilling out on the existing wellbore (kick-off point) to a new termination point for the well[45].

Multilateral wells: Multilateral wells have more than one wellbore radiating from the main wellbore[45]. In contrast to sidetracked wells, where the first bottom section is plugged back before a sidetrack is drilled, multilateral wellbores have more than one wellbore open at the same time[45]. **Active wells:** Operating-/active wells are defined as production or injection wells that are currently producing or injecting[45].

Abandoned wells: Inactive wells may be temporarily or permanently abandoned. According to the regulations of the NORSOK D-010 standard[3], temporarily abandoned wells are defined as all wells/ wellbores except all active wells and wells that are permanently plugged and abandoned (P&A). Temporarily abandoned wells can be sealed with a mechanical plug, whereas permanently plugged and abandoned wells, whose casings and wellhead need to be cut-off at least 5 mbsf, are sealed with cement[3].

2. Supporting Material and Methods

2.1 Geochemical and seismic data analysis of CH_4 leakage at three abandoned gas wells in the Central North Sea

The following section provides a summary of relevant geochemical and seismic analysis of three leaky abandoned wells (15/9-13, 16/4-2, and 16/7-2) located in water depths of 81-93 m in the Norwegian CNS (Figure 2), earlier published by Vielstädte et al.[20]. The authors[20] characterized the origin of the emanating gases (2.1.1), leakage rates (2.1.2), and initial gas bubble size distribution (2.1.) providing a baseline for the extrapolation analysis presented in this study. Sections 2.1.4 and 2.1.5 include new geochemical data on CH_4 oxidation rates in the water column observed at wells 15/9-13 and 16/7-2 and total organic carbon (TOC) and sulfate (SO_4) concentrations in near surface sediments at a reference site in the CNS, respectively.
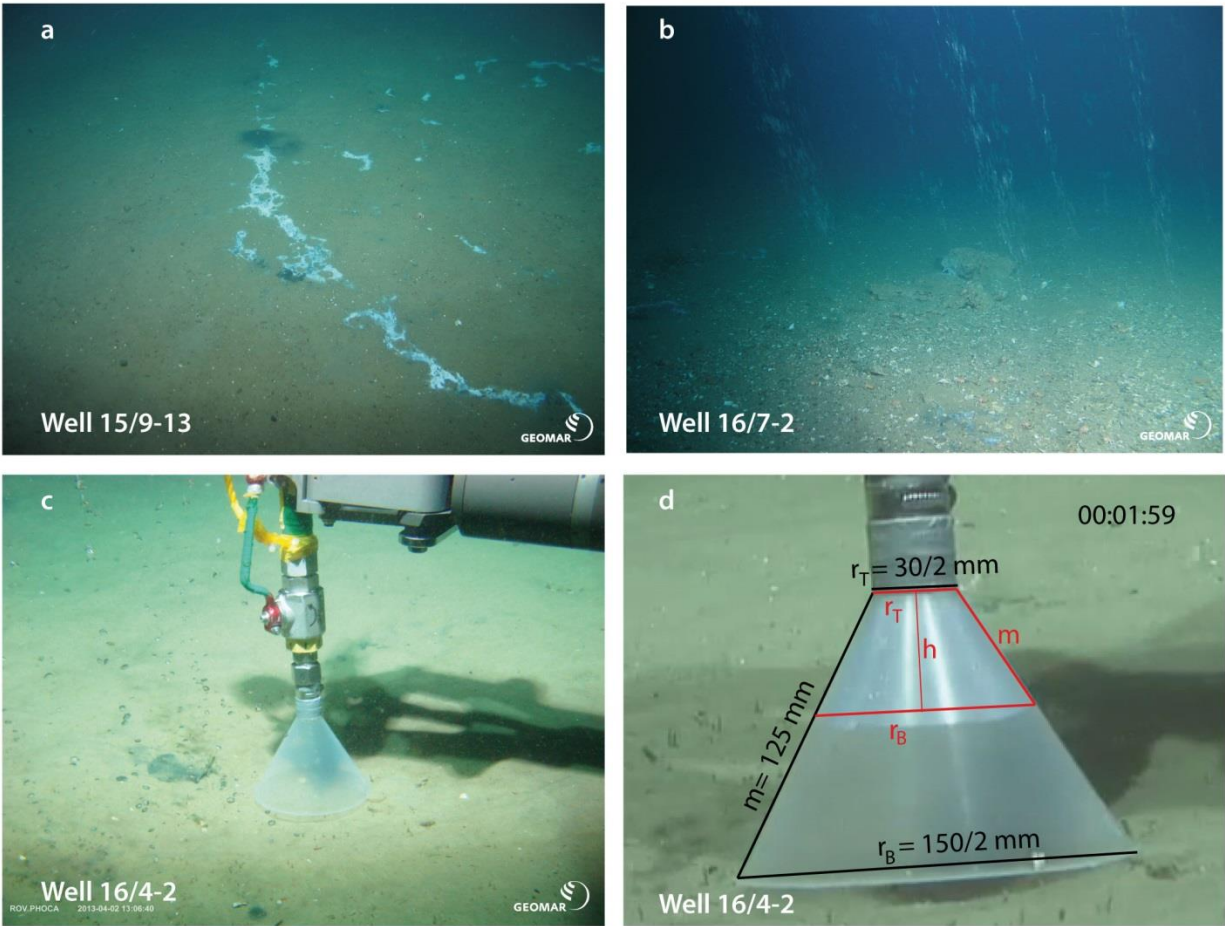
Figure S1| Gas leakage and gas flow measurements at the three wells investigated in Reference[20] (note that plugging and abandonment regulations in the North Sea require the cut-off of wellheads at least 5 m below the seafloor, so that these wells "disappear"). Pictures showing **a)** bacterial mats related to CH_4 leakage at well 15/9-13, **b)** the most intense leakage at well 16/7-2, **c)** gas flow measurement at well 16/4-2, and **d)** exemplary visualization of optically derived gas flow measurement at well 16/4-2 using the funnel attached to the gas sampler. Dimensions of the funnel are: m = lateral funnel height, r_T = radius of the top plane, and r_B = radius of the bottom plane. The gas volume was determined by measuring the corresponding dimensions of the gas filled frustum of a cone and calculating the height, h (red letters) as described in Reference[20].

2.1.1 Determining the origin of leaking gases. The origin of the leaking gases was analyzed by Vielstädte et al.[20] combining geochemical and seismic investigations at the three leaky abandoned

wells (15/9-13, 16/4-2, and 16/7-2) in the Norwegian Sector of the CNS (Figure 2). Full methodological detail on the geochemical analysis of free seep gases and porewaters at the three investigated wells is given in Reference[20]. Figure S2 shows the results.
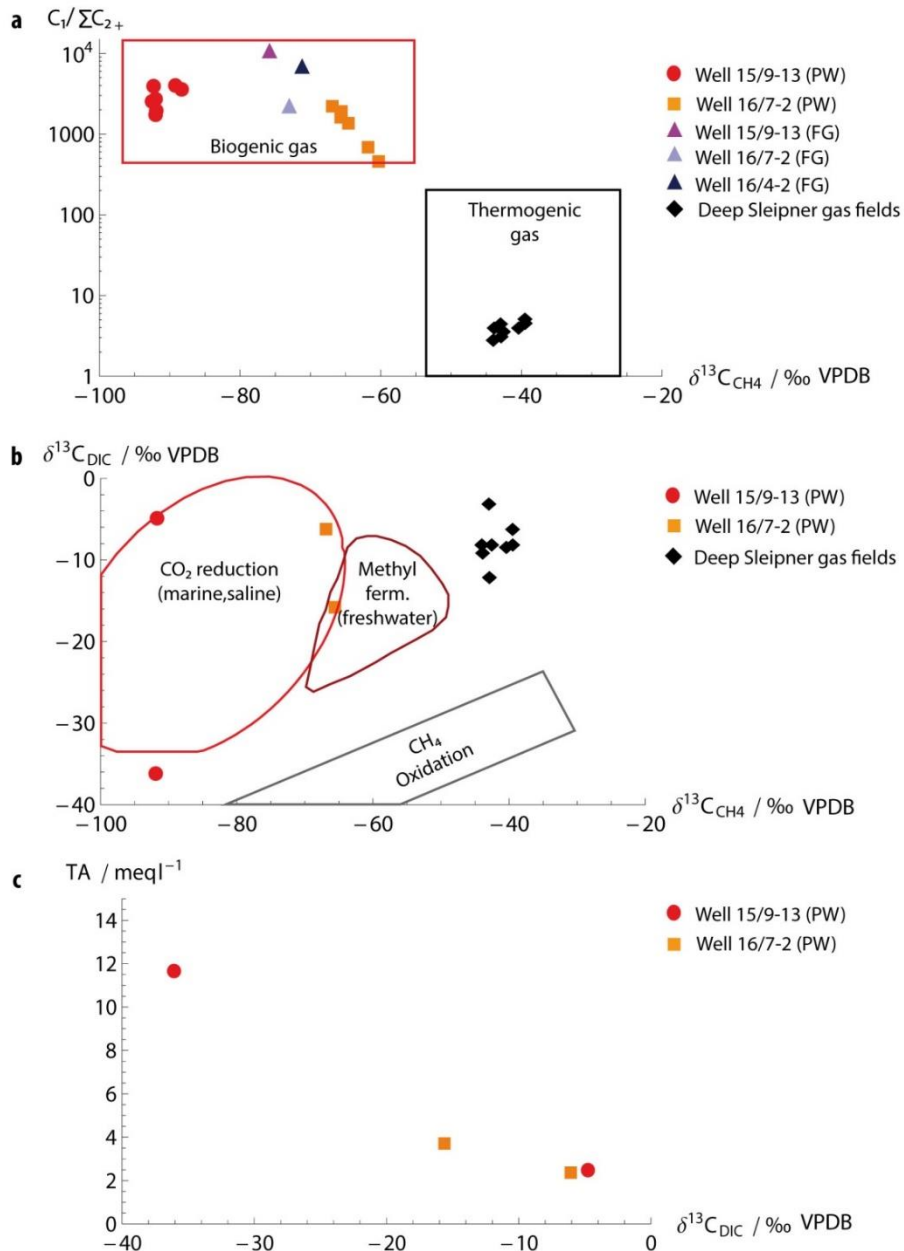

Figure S2| Results of geochemical analysis of free seep gases and porewaters at the three investigated wells (as published by Vielstädte et al.[20]). (**a**) Bernard diagram of the molecular and

isotopic gas composition (after Bernard et al.[48]) indicating the gas source of the gas at the abandoned wells (red dots: porewater (PW) at well 15/9-13, orange rectangle: porewater at well 16/7-2, triangles: free seep gas (FG) at wells 15/9-13, 16/7-2, and 16/4-2) and the deep hydrocarbon reservoirs in the area (black diamonds [49]). (**b**) Cross-plot of $\delta^{13}C$ of DIC versus $\delta^{13}C$ of CH_4 in the porewater at well 16/7-2 (orange rectangles), well 15/9-13 (red dots), and the deep hydrocarbon reservoirs (black diamonds)[49]. (**c**) Cross-plot of total alkalinity (TA) and $\delta^{13}C$ of DIC indicating microbial anaerobic oxidation of CH_4.

In addition to geochemical analysis, Vielstädte et al.[20] analyzed industrial 3-D seismic data (ST98M3, Statoil ASA) for shallow gas pockets in the area around the three wells by mapping high amplitude anomalies[22] in the upper 1000 m of sediment using Petrel (Schlumberger). The locations of identified gas pockets were assigned to stratigraphic units[24] and correlated with the well-paths of the three leaky wells. The authors[20] found that two of the wells (i.e. 15/9-13 and 16/7-2) have been drilled through shallow gas in Lower Pliocene (LP) and Top Pliocene (TP) stratigraphic units (Figure 2 b). For well 16/4-2, the seismic data did not reveal prominent bright spots (i.e. reverse polarity high amplitude anomalies) in the direct vicinity of the well-path, indicating that leakage at well 16/4-2 draws gas from larger distances (spatial resolution of the seismic data is ~10 m). Additionally, seismic turbidity in near-surface sediments (Figure 2 b, 0.1 – 0.4 s two-way-travel time TWT) might indicate an unfocussed distribution of gas[50].

2.1.2 Quantifying per-well leakage rates. The *in-situ* gas flow was quantified at single bubble streams (here referred to as seeps) of wells 16/4-2 and 15/9-13 using the ROV-operated gas sampler with attached funnel (Figure S1 c,d) as described in Reference[20]. At well 16/7-2, the *in-situ* gas flow was derived from bubble size measurements[20]. Each flow measurement lasted about 10 minutes, thus temporal variations in the gas flux on time-scales longer than that remain unknown. Longer time-series will be necessary to better constrain our annual emission estimates. Table S1 comprises data of gas flow measurements at the three wells investigated by Vielstädte et al.[20].

Here, the gas flow measurements at wells 15/9-13 and 16/4-2[20] were used for the assessment of the North Sea-wide release assignment. We only considered the two lower gas flows measured at wells 15/9-13 and 16/4-2[20] because they are believed to be more typical for shallow gas migration than the larger gas flow measured at well 16/7-2, which has been drilled through a seismic chimney[20].

Table S1| Quantification of seabed gas releases along three abandoned wells in the Central North Sea (compiled data based on Vielstädte et al.[20]; a seep here refers to as a single bubble stream).

Well (Water-depth)	Q_{SF} (*in-situ*) / L min^{-1} seep^{-1} of CH_4	Q_{SF} (STP) / L min^{-1} seep^{-1} of CH_4	No. of seeps	Q_{SF}[a] / t yr^{-1} well^{-1} of CH_4
15/9-13 (81 mbsl)	0.09	0.9[f]	2	1
16/4-2 (93 mbsl)	0.15 /0.17[b]	1.6/1.8[b,d]	8	4
16/7-2 (83 mbsl)	0.15[c]	1.4[e]	39	19

[a] based on the average gas flow of 1.4 L min^{-1} seep^{-1} at STP (35 PSU, 25°C, 1 bar)

[b] based on replicate gas flux measurements at well 16/4-2

[c] derived from bubble size, due to lack of direct funnel measurements

[d] measured at high tide

[e] measured at low tide

[f] measured 2 h after low tide

2.1.3 Measuring initial bubble sizes. Vielstädte et al.[20] analyzed initial bubble size spectra at the three wells from ROV-video sequences applying the image editing software ImageJ[51]. For each bubble, the major and minor axes, angle, perimeter, area, circularity, as well as frame number were recorded. The corresponding bubble volume, $V_0=4/3\pi \times r_e^3$, was calculated from the equivalent spherical radius, $r_e= (a^2b)^{1/3}$ based on the major, a, and the minor half axes, b, of the fitted ellipse as described in Reference[20].

Determined bubble sizes at wells 15/9-13 and 16/4-2 were combined into a common bubble size distribution (ψ)[20] (Figure S5). Given that the gas flow at individual seeps of the wells was low such that initial bubble formation processes are primarily controlled by the mechanical properties of the surface sediments [38], ψ is proposed to be representative for bubbles released from the fine to medium-grained clayey sand found at the investigated wells and in wide areas of the North Sea[26]. The combined bubble size distribution (ψ)[20] was thus, used for further extrapolation of CH_4 leakage to the North Sea scale by calculating the fate of leaking CH_4 from the seafloor to the atmosphere using a numerical bubble dissolution model (SI Section 2.2.2).

Measurements at well 16/7-2 were excluded for the determination of the combined bubble size distribution because bubbles escaped from below a carbonate rock, thereby expelling significantly larger bubbles into the water column than bubbles directly released from the sandy sediments (i.e. at well 15/9-13 and 16/4-2, for details see Reference[20]).

2.1.4 Quantifying dissolved CH_4 and CH_4 oxidation (MOx) rates in the water column. During cruise CE12010 (July-August 2012), seawater samples were taken with Niskin bottles attached to a video-guided CTD or operated by ROV Kiel 6000[53]. At wells 15/9-13 and 16/7-2 seawater was sampled near the seafloor and additionally through the water column at well 15/9-13. No water samples were recovered at well 16/4-2. For dissolved gas analysis, subsamples were transferred bubble-free into 100 ml headspace vials immediately after recovery of the Niskin Water Sampler Rosette. Dissolved gases were released from the seawater samples by headspace technique (headspace of 10 ml of Ar 4.5). After adding 50µl of saturated $HgCl_2$-solution the vials were stored at 4°C. Concentration determination of CH_4 released into the headspace was conducted by using onboard gas chromatography (Shimadzu 2010, for results see Table 1 and Figure S3).
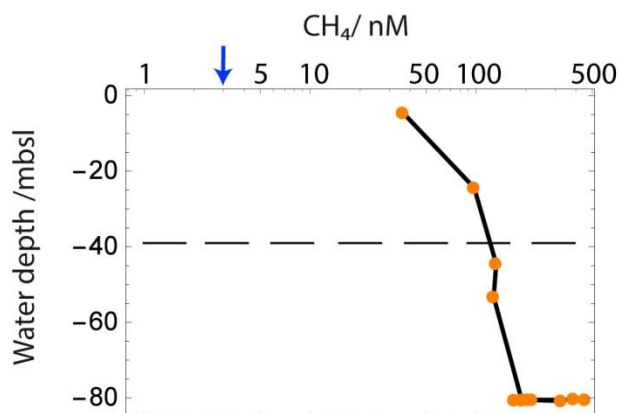
Figure S3| Dissolved CH$_4$ concentrations in the water column. Depth profile showing the concentration of dissolved CH$_4$ in the water column (orange bullets) based on measurements during CE12010 31-CTD7 at well 15/9-13. The dashed line indicates the depth of the thermocline and the blue arrow represents the equilibrium concentration of CH$_4$ in the surface mixed layer (i.e. 3 nM[30]) with respect to the atmospheric partial pressure of CH$_4$.

To assess CH$_4$ oxidation rates (r_{MOx}) in the water column, subsamples were transferred bubble-free into ~23 ml headspace vials and closed with grey bromo-butyl stoppers (Helvoet Pharma, Belgium), immediately after recovery of the Niskin bottles. Shortly after sampling, a 6 µl gas bubble of ^{14}C-CH$_4$:N$_2$ gas (0.25 kBq) was added to the subsamples, which were then incubated for 2 days in the dark at *in-situ* temperature (~8°C). After 2 days, samples were fixed in 4 pellets of NaOH and stored at 4°C until rate measurements were performed in the home laboratory. Radioactive substrate and product pools were quantified as described by Blees and colleagues[54-55] to determine the rate constant. Assuming sufficient oxygen supply during incubation, CH$_4$ oxidation rates were then calculated according to:

$r_{MOx} = k \times [CH_4]$ Supplement Eq. (1)

where k is the first-order rate constant and [CH$_4$] denotes the concentration of CH$_4$ in seawater (for results see Table 1). All rates were determined in quadruplicates. Killed controls (addition of 200 µl saturated HgCl$_2$ at the start of the incubation) were analyzed for each incubation period. Recovery of the radioactive tracer was >95%. The detection limit of the rate depends on the amount of radioactive CH$_4$ added and the initial CH$_4$ concentration and varied between 0.01 and 6.45 nM day^{-1} depending on the sample. Above well 15/9-13, all rates were below detection limit. Above well 16/7-2, one out of three sampling locations showed rates below detection limit. For the other two locations above well 16/7-2, rates were 0.19±0.07 and 1.40±0.83 nM day^{-1} (SEM, N=4).

For comparison, maximal MOx rates measured at well 16/7-2 were generally one order of magnitude lower than those observed at other highly active natural marine seep sites (e.g. at hydrothermal vents at the Juan de Fuca Ridge[56], cold seeps in the Santa Barbara Channel[57] at Hydrate Ridge[58] and the Svalbard continental margin[39]), and 2-3 orders of magnitude lower than at other, more catastrophic anthropogenic methane release sites (e.g. the Deep Water Horizon oil spill where MOx rates were $\leq$5900 nM d^{-1} [59] and the North Sea Blowout well 22/4b where MOx rates were $\leq$498 nM d^{-1} [40]). Even though CH_4 concentrations were high throughout the water column (i.e. 36-1014 nM at well 15/9-13) and there was no limitation in O_2, the low activity of microbial CH_4 oxidation at the investigated wells may be due to changes in the abundance of CH_4 oxidizing bacteria (MOB) caused by water mass exchange. Steinle et al.[39] found that lateral transport of water column MOB away from the CH_4 point source reduced water column MOx activity at seeps offshore Svalbard. A similar impact of lateral transport was found at the Blowout well 22/4b in the British Sector of the North Sea, were MOx rates were significantly higher within the seabed crater which was partly shielded against tidal influences and currents[40].

2.1.5 Quantifying total organic carbon (TOC) and dissolved sulfate (SO$_4$) concentrations in surface sediments and associated pore fluids. In summer 2012, surface sediment samples were retrieved in the CNS using the Geo-Corer 6000 vibro corer (VC) system provided by the Geological Survey of Ireland[53]. VC sediment cores were cut in half and ~3 cm thick slices were taken in approximately 20-40 cm intervals. Subsequently, the porewater was extracted at ambient room temperature (~19°C) using a low pressure-squeezer (argon at 3-5 bar, sometimes up to 7 bar). While squeezing, the porewater was filtered through 0.45 μm regenerated cellulose Whatman filters and collected in recipient vessels. Concentration determination of SO$_4$ in pore fluids and TOC in the sediment was conducted from subsamples using shore-based ion chromatography (METROHM 761 Compact IC-System) and the CARLO ERBA Elemental Analyzer (NA 1500, operating at 1050°C), respectively. TOC measurements in the sediment were made in ~10 cm intervals using freeze-dried and grinded subsamples that were weighed into silver cups and acidified with 0.25N hydrochloric acid to remove carbonate carbon, prior to combustion.

The low TOC concentrations in surface sediments (~0.1 wt %) and high dissolved SO_4 concentrations in associated pore fluids (29 mM) document the low potential for biogenic gas formation in CNS surface sediments (see Figure S4). These geochemical observations confirm that the biogenic gas emitted at the wells does not originate from microbial gas production in ambient surface sediments but from subsurface gas reservoirs.
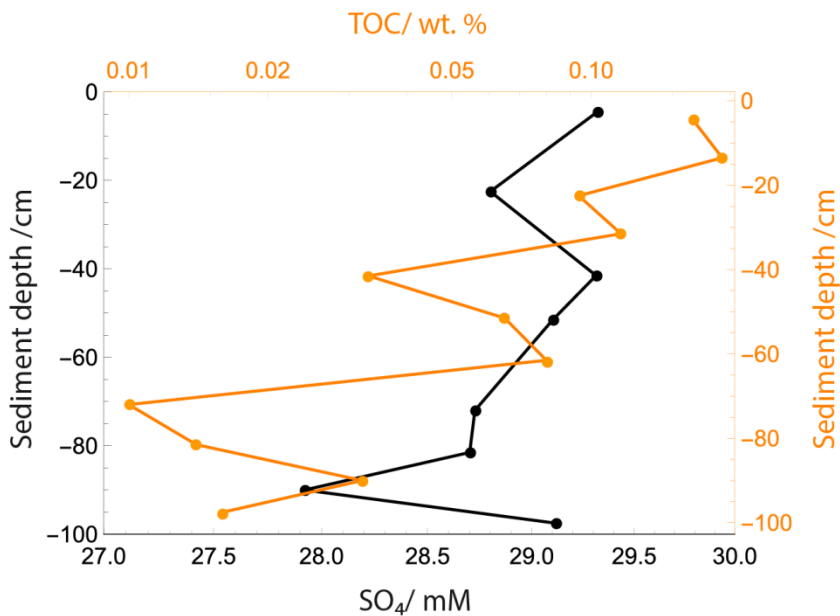

Figure S4| Total organic carbon (TOC) and dissolved sulfate (SO_4) concentrations in the sediment. Depth profile showing the concentrations of TOC (orange bullets) and dissolved SO_4 (black bullets) in the CNS surface sediments based on measurements at a reference station in 88.6 m water depth (CE12010 18-VC7, 58°35.740'N, 02°05.179'E). Similar values were measured in other sediment cores taken during cruise CE12010.

2.2   Extrapolation of drilling-induced CH$_4$ leakage to the North Sea scale

2.2.1 Seismic mapping of shallow gas and the probability of wells to leak. The examination of the probability of wells to leak shallow gas is based on the analysis of an industrial 3-D seismic data set ST98M3, which is the result of merging seven independently acquired and processed sub-datasets. Detailed information regarding processing parameters of the specific subsets are not available, while the processing sequence for merging the data included resampling, filtering, phase rotation and amplitude adjustments. The final 3-D seismic cube shows positive acoustic

impedance contrasts as positive amplitude (blue) followed by negative amplitude (yellow). The bin-size is 12.5 m and the vertical resolution is ~10 m (dominant frequency 45 Hz, seismic velocity of ~1800 m/s for the upper 400 m and ~2000 m/s below). The dataset extends 62 km from north to south and 46 km from east to west covering an area of more than 2000 km² (Figure 2 a).

Shallow gas pockets in the uppermost 1000 m of sediment, identified by high amplitude anomalies in the seismic data[22], were mapped and assigned to stratigraphic units[24] using the seismic analysis software Petrel (Schlumberger). Assuming that leakage of shallow gas can potentially occur along any type of well (producing, injecting, abandoned, dry), as long as there is a shallow gas accumulation in its vicinity, an increased permeability induced by the drilling operation, and a driving force for gas movement, which could be buoyancy or excess pore pressure, we correlated the well paths of a total of 55 wells in the seismic study area with locations of shallow gas pockets. 50 sidetracked and multilateral wells were excluded for the correlation analysis because they separate from the main well in the deeper subsurface, which was not the scope of this study. Further, 55 wells, having platforms at the sea surface, were deselected because no 3-D seismic data of the overburden sediments existed. The probability of wells to leak shallow gas was then determined by the fraction of wells which penetrate high amplitude anomalies in the shallow subsurface (i.e. 18 of 55 selected wells, Figure 2) and is required for further extrapolation of CH_4 leakage to the North Sea scale (SI Section 2.2.4).

2.2.2 Modeling the fate of leaking CH_4. An existing numerical bubble dissolution model[20] was used to calculate the bubble-mediated CH_4 flow to the atmosphere by a single rising gas bubble. The simulation of a single rising bubble seems to be justified because only single bubble streams were observed at the investigated wells (Figure S1) with very little to no interaction between the bubbles, or plume dynamics (upwelling). Assuming that the release of single bubble streams is representative for leaky wells in the North Sea, the model simulates the shrinking of a gas bubble due to dissolution in the water column, its expansion due to decreasing hydrostatic pressure in the course of its ascent and gas stripping, and the final gas transport to the atmosphere. A set of coupled ordinary differential equations (ODEs) was solved numerically describing these processes for each of the involved gas species (CH_4, N_2, and O_2; Eq. S2) and the bubble rise

velocity (Eq. S3), thus time being the only independent variable. Thermodynamic and transport properties of the gas components, such as molar volume, gas compressibility, and gas solubility in seawater, were calculated from respective equations of state[60-63], and empirical equations for diffusion coefficients[64], mass transfer coefficients[65], and bubble rise velocities[66], taking into account local pressure, temperature and salinity conditions as measured by CTD casts. Implemented equations and values are provided in Table S2. The ODE system is solved using finite difference methods implemented in the NDSolve object of Mathematica (i.e. LSODA)[67].

The mass exchange of gas components across the bubble surface is generally described as[66, 68-69].

$$dN_i / dt = 4\pi r_{eq}^2 \ K_{L,i} \ (C_{a,i} - C_{eq,i})$$ Supplement Eq. (2)

where i is the ith gas species, N, is the amount of gas in the bubble, $4\pi r_{eq}^2$ is the surface area of the equivalent spherical bubble, K_L is the specific mass transfer rate between gas phase and aqueous phase, C_a is the dissolved gas concentration, and C_{eq} is the gas solubility. All of the above variables are functions of the water depth, z, i.e. pressure, temperature and salinity (see Table S2 for details and references). The change of the vertical bubble position is related to the bubble rise velocity, v_b (Table S2):

$$dz / dt = v_b$$ Supplement Eq. (3)

Model simulations were performed based on boundary conditions obtained in the CNS from Sea-Bird 9 plus CTD data of August 2012 (Table S2) and run for different initial bubble sizes (ranging between 1.0 to 4.0 mm radius, in accordance to radii of the combined bubble size distribution, SI Section 2.1.3), initially containing only CH_4. Simulated water depths ranged between 20 and 150 m in accordance to those important for the CH_4 bubble transport to the surface mixed layer (SML) of the North Sea. Larger water depths were not considered because additional model runs revealed that the combined bubble size distribution completely loses its initial CH_4 content in the deep layer of the North Sea when released from more than 150 m depth, Figure S5.

The CH_4 emissions from leaky wells to the atmosphere were calculated distinguishing between direct emissions via bubble transport and indirect emissions via the diffusive outgassing of CH_4 dissolving in the SML (i.e. the upper 50 m of the North Sea water column)[37]. The direct bubble

CH$_4$ transport to the atmosphere was calculated from the remaining/residual amount of CH$_4$ in the bubble, when it reaches the sea surface, N_S, i.e.

$$N_S(r,z) = N_0(r,z) - \int_{t=0}^{tmax} dN(r,z)\, dt$$

Supplement Eq. (4)

,where N_0 is the initial amount of CH$_4$ in the bubble and *tmax* is the time required by the gas bubble to travel to the sea surface and is determined numerically by the bubble dissolution model. The amount of CH$_4$ dissolving in the SML of the North Sea (N_{SML}) was calculated by integrating the rate of CH$_4$ bubble dissolution over the time which is needed by the bubble to travel through the upper 50 m of the water column (i.e. t_{50} to *tmax*, both determined numerically by the bubble dissolution model):

$$N_{SML}(r,z) = \int_{t50}^{tmax} dN(r,z)\, dt$$

Supplement Eq. (5)

Both, the residual CH$_4$ and the CH$_4$ dissolving in the SML depend on the initial bubble size (r) and water depth (z) and were normalized to the corresponding N_0. The relative amount of CH$_4$ at the sea surface and in the SML with respect to the initial bubble CH$_4$ content, i.e. $\Omega_S(r,z) = N_S(r,z) / N_0(r,z)$ and $\Omega_{SML}(r,z) = N_{SML}(r,z) / N_0(r,z)$, are referred to as the transport efficiencies of a single gas bubble to the sea surface and to the SML, respectively.

A transfer function was fitted to numerical results using the non-linear least-squares fit algorithm. The fit describes the CH$_4$ transport efficiency of a single bubble to the sea surface as a function of the initial bubble size (r) and the leakage depth (z):

$$\Omega_S(r,z) = e^{-\frac{a}{r^b}z}$$

Supplement Eq. (6)

	Correlation matrix for parameters		Least squares estimates of parameters	Standard deviation (1-σ)
	a	b		
a	1	-0.97	-0.156	0.007
b	-0.97	1	1.26	0.04

The variance, s^2 of the residuals is better than 0.00013 and the linear correlation coefficient of the fit-curve to the numerical data is better than 0.99. The fit function is valid for initial bubble radii ranging between 1 and 4 mm initially containing only CH_4 and for the given physicochemical properties of the water column obtained in the CNS from Sea-Bird 9 plus CTD data of August 2012 (Table S2). By applying Supplementary Eq. 6, the mass transfer of gases other than CH_4, N_2, and O_2, as well as the development of upwelling flows are considered to be negligible for the CH_4 transport to the sea surface.

Because leaky wells expelled a range of initial bubble sizes, the transport efficiencies $\Omega_S(r,z)$ and $\Omega_{SML}(r,z)$ were calculated for each bubble size and weighted by its volumetric contribution, V_0, to the total emitted gas bubble volume, V_ψ. Integrating this weighted bubble transport efficiencies over the entire bubble size spectrum (ψ) gives the total CH_4 transport efficiency to the SML (Ω_{SML}) and to the sea surface (Ω_S) with respect to the initial CH_4 release at the seafloor, respectively:

$$\Omega_S(\psi,z) = \frac{1}{MI} \int_{r(min)}^{r(max)} \Omega_S(r,z) \, \frac{V_0(r)}{V_\psi} \, dr \qquad \text{Supplement Eq. (7)}$$

$$\text{Supplement Eq. (8)}$$
$$\Omega_{SML}(\psi,z) = \frac{1}{MI} \int_{r(min)}^{r(max)} \Omega_{SML}(r,z) \, \frac{V_0(r)}{V_\psi} \, dr$$

where, $r(min)$, and $r(max)$ are the minimum and maximum radii of the bubble size spectrum ψ[20], respectively, and MI is the measurement interval between individual bubble sizes (i.e. 0.1 mm). V_0 and V_ψ refer to optical size measurements at individual gas streams of the investigated wells, which were conducted to determine the combined bubble size spectrum[20] (Figure S5). Applying Supplementary Eq. 7 and 8, we assume that there is no change in the weighted volumetric contribution of each bubble size to the total emitted bubble volume (i.e. $V_0(r) / V_\psi = const.$), so that the relative distribution of bubble sizes is considered to be constant, although the release frequency of bubbles may change due to a variability of the seabed gas flow. This means that at a constant mass flow (i.e. per-well leakage rate) a decrease in the hydrostatic pressure (i.e. leakage depth) increases the rate of bubble formation but not their size distribution, as generally validated for seeps with a low gas flow[38]. Transfer functions were fitted to numerical results of Supplementary Equation 7 and 8, respectively using the non-linear least-squares fitting algorithm "NonlinearModelFit" of Mathematica (Figure S5). The fit-curves describe the transport

efficiency of the bubble size distribution to the sea surface (Eq. S9) and to the SML (Eq. S10) with respect to the seabed CH_4 flow and as a function of the leakage depth (z), respectively:

$$\Omega_S(\psi,z) = e^{-a \cdot z} \qquad\qquad \text{Supplement Eq. (9)}$$

Parameter	Least squares estimates of parameter	Standard deviation (1-σ)
a	0.0435	0.0007

$$\Omega_{SML}(\psi, z) = \frac{1}{1 + e^{z-50}} \, a \times z^{0.5} + \frac{1}{1 + e^{50-z}} \qquad \text{Supplement Eq. (10)}$$
$$\times \frac{1}{b + c \times z^{4.6}}$$

	Correlation matrix for parameters			Least squares estimates of parameters	Standard deviation (1-σ)
	a	b	c		
a	1	0.3	-0.2	0.127	0.003
b	0.3	1	-0.8	0.73	0.04
c	-0.2	-0.8	1	6.1×10^{-9}	4×10^{-10}

The variance, s^2, of the fits is 0.0001 and 0.0005 for the transport efficiency to the sea surface and to the SML, respectively. The numerical accuracy of the model, determined from mass balance errors, was overall better than 99.9%. Supplementary Eq. 9 and 10 are required for the North Sea-wide extrapolation of drilling-induced CH_4 emissions from the seafloor into the atmosphere (SI Section 2.2.4).

Table S2| Parameterization of numerical model.

Parameterization	Range	Variance	Reference
[a] Diffusion coeff.: D_i / m^2 s^{-1}			
$D_{O2}=1.05667\times10^{-9}+4.24\times10^{-11}\times T$	T:0-25°C	1.00×10^{-21}	Boudreau[64]
$D_{N2}=8.73762\times10^{-10}+3.92857\times10^{-11}\times T$	T:0-25°C	2.94×10^{-23}	Boudreau[64]
$D_{CH4}=7.29762\times10^{-10}+3.31657\times10^{-11}\times T$	T:0-25°C	5.70×10^{-24}	Boudreau[64]
Mass transfer coefficient: $K_{L,i}$ / m s^{-1}			
$K_L=0.013(v_b\times10^2/(0.45+0.4\ r\times10^2))^{0.5}\times D_i^{\ 0.5}$	r≤ 2.5 mm		Zheng and Yapa[65]
$K_L=0.0694\times D_i^{\ 0.5}$	2.5< r ≤ 6.5 mm		Zheng and Yapa[65]
$K_L=0.0694\ (2r\times10^{-2})^{-0.25}\times D_i^{0.5}$	r< 6.5 mm		Zheng and Yapa[65]
Fit to CTD data as function of z			
$T(z)=8+7/(1+e^{\ 0.375\ (-21.7512+z)})$	Z: 0-150 m	3.99×10^{-2}	
$S(z)=35.12-0.67/(1+e^{\ 0.4125\ (-20.1595+z)})$	Z: 0-150 m	4.97×10^{-4}	
Density of SW: φ_{SW}/ kg m^{-3}			
$\varphi_{SW}(z)=1027.7-2.150/(1+e^{\ 0.279\ (-21.612+z)})$	Z: 0-150 m	6.8×10^{-3}	Unesco[70]
Bubble rise velocity: vb / m s^{-1}			
$v_b=4474\times r^{1.357}$	r< 0.7 mm		Wüest et al.[66]
$v_b=0.23$	0.7≤ r < 5.1 mm		Wüest et al.[66]
$v_b=4.202\times r^{0.547}$	r≥ 5.1 mm		Wüest et al.[66]
Gas solubility: c_i / mM			
$cN2=0.622+0.0721\ z$	Z:0-150 m	2.5×10^{-3}	Mao and Duan[63]
$cO2=1.08+0.1428\ z$	Z:0-150 m	9.8×10^{-3}	Geng and Duan[62]
$cCH4=1.44+0.1671\ z$	Z:0-150 m	2.4×10^{-2}	Duan and Mao[61]

CH$_4$ molar volume: MV_{CH4} / L mol^{-1}

$MV_{CH4}=1/(0.0418+0.0044\ z)$ Z:0-150 m 3.0×10^{-2} Duan et al.[60]

Hydrostatic Pressure: P_{hydro}/ bar

$P_{hydro}=1.013 + \varphi_{SW} \times g \times z$

---

[a] *The parameterization of the diffusion coefficients is based on a seawater salinity of 35 PSU. Pressure effects have been neglected because at the given water depths (<150 m) the resulting error is less than 1%.*
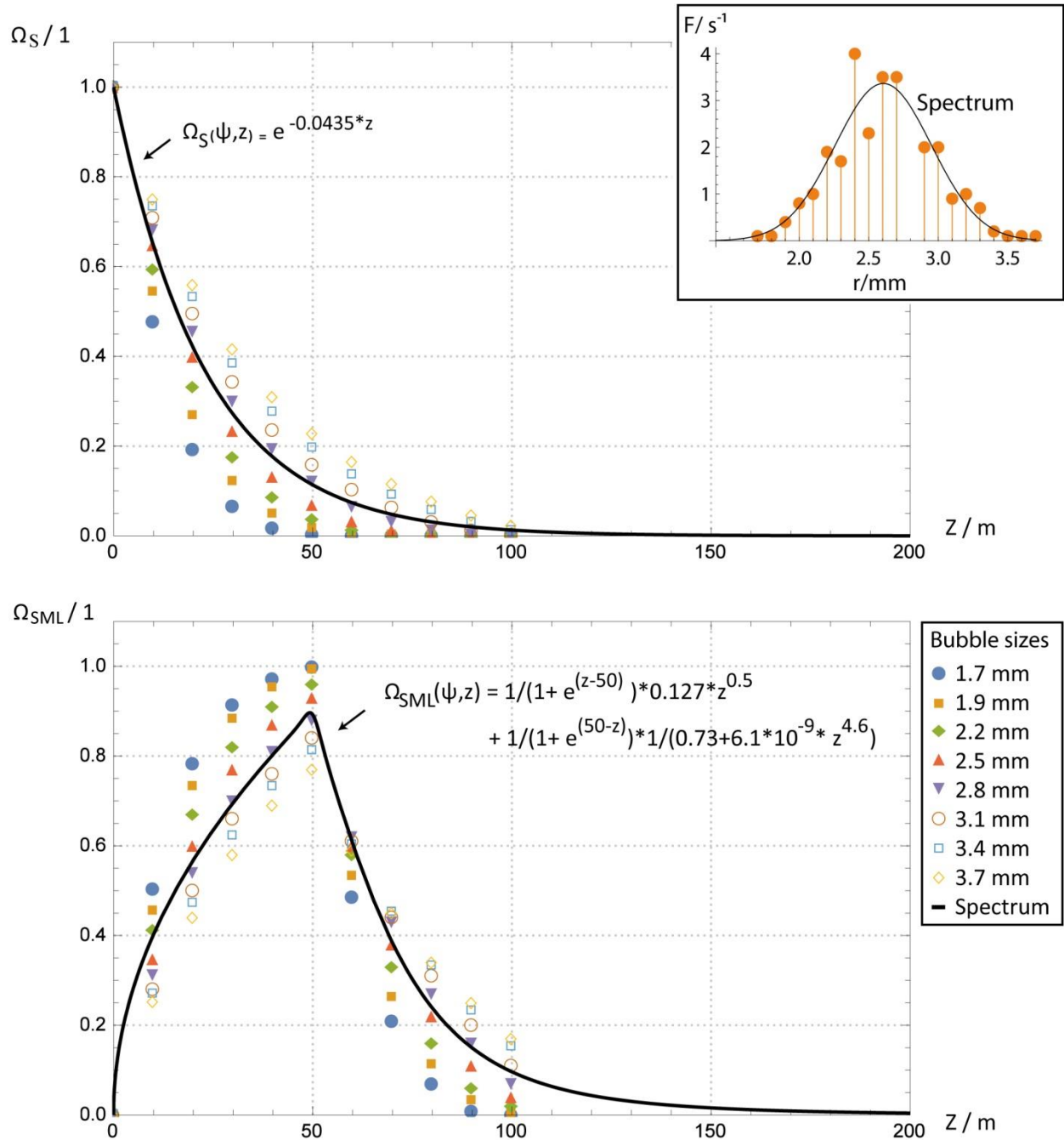
Figure S5| Numerical results of the bubble dissolution model. Model results show the CH_4 bubble transport efficiency to the surface mixed layer (Ω_{SML}) and to the sea surface (Ω_S) of the North Sea, respectively as a function of the leakage depth (z) and for initial bubble radii ranging between 1.7 to 3.7 mm (in accordance to bubble sizes of the combined bubble size distribution measured at the three investigated leaky wells[20]; upper right corner showing the measured bubble release frequency (F) versus bubble radius (r), and Gaussian fit (black line) for the combined

bubble size spectrum[20]). The CH$_4$ transport efficiency of the combined bubble size distribution (black curve) was determined by fit curves to the data using the non-linear least-squares fitting algorithm "NonlinearModelFit" of Mathematica. The variance, s^2, of the fit-curves is better than 0.001 and 0.005 for $\Omega_S(\psi,z)$ and $\Omega_{SML}(\psi,z)$, respectively.

2.2.3 The well inventory and bathymetry of the North Sea. To extrapolate CH$_4$ leakage to the North Sea scale, all 15 781 offshore wellbore data (including the well identification, location, status, and type) were incorporated into a database created in ArcGIS (v10.1), sourced from online datasets published by governmental energy departments and regulation agencies in 2012 to 2013 (Table S3, Figure S6). Filters (queries) were applied to categorize and identify the wells for analysis (Table S4). As leakage of shallow gas can potentially occur along any type of well, whether it is producing hydrocarbons, injecting fluid into a reservoir, was dry, or has been abandoned, we selected all types of wells (i.e. 11 122 wells, see Table S4), excluding extra sidetracked and multilateral wells which tend to separate from the main well in the deeper subsurface (i.e. < 1000 m). Sidetracked and multilateral wells were deselected manually from the database following the guidelines for designation of wells and wellbores[45]. In addition, the EMODnet North Sea bathymetry with a spatial resolution of 5 minutes (available at: http://www.emodnet-bathymetry.eu; Figure S6) was incorporated into the ArcGIS database. Bathymetric data were required to estimate CH$_4$ emissions into the atmosphere, which are depth-dependent.

Table S3| Source data of the North Sea well inventory.

Country	Data Source (Date)	Link
Norway	Norwegian Petroleum Directorate (Sept. 2013)	http://factpages.npd.no/ReportServer?/FactPages/geography/geography_all&rs:Command=Render&rc:Toolbar=false&rc:Parameters=f&IpAddress=1&CultureCode=en
United Kingdom	Department of Energy and Climate Change (Aug. 2013)	https://www.gov.uk/oil-and-gas-offshore-maps-and-

gis-shapefiles

Germany	Niedersächsisches Landesamt für Bergbau, Energie und Geologie (Jul. 2013)	http://nibis.lbeg.de/cardomap3/?TH=BOHRKW
Denmark	Danish Energy Agency (Jan. 2012)	http://www.ens.dk/en/oil-gas/oil-gas-related-data/wells
Netherland	Netherland Oil and Gas Portal (Jun. 2013)	http://www.nlog.nl/en/activity/activity.html

Table S4| Classification of wells in the North Sea (as of 2012-2013).

Well Status	Main Wells/Wellheads	Additional sidetracked & multilateral wells	Total number
Active[a]	2818	1629	4447
Inactive[b]	7498	2637	10 135
Shut-in[c]	5636	1696	7332
Unknown status[d]	806	393	1199
Total	11 122[e]	4659	15 781

[a] *including injection, production, and open wells*

[b] *including temporarily and permanently plugged and abandoned wells*

[c] *including only permanently plugged and abandoned/ shut-in wells; excluding wells in the Danish Sector because here no well status was reported in the source data*

[d] *including wells where no well status or type was reported, and Norwegian wells which have been completed to well, or predrilled with no further specification*
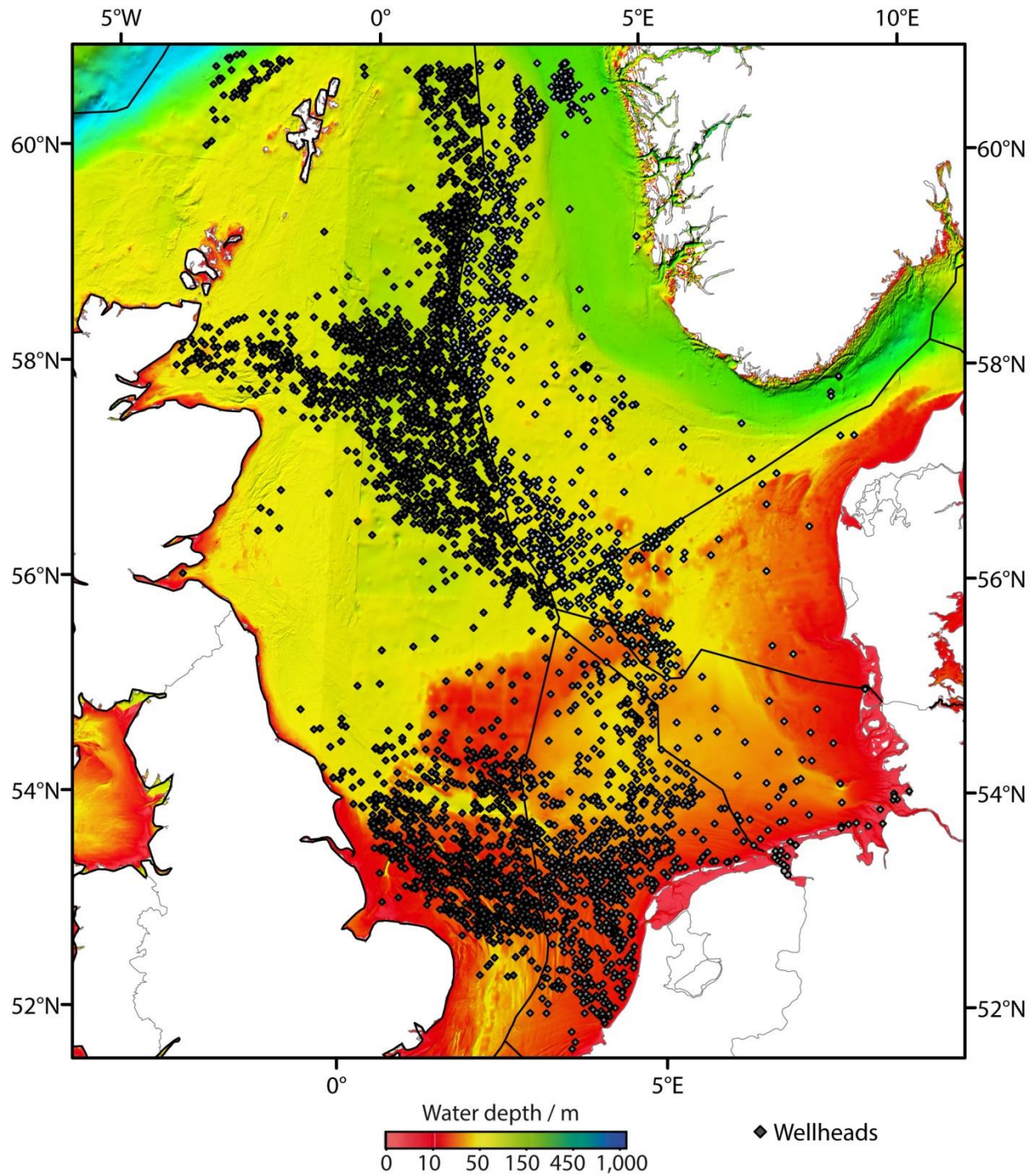
[e] *selected for analysis*

Figure S6| Bathymetric map of the North Sea and the surface location of the 11 122 wells (grayish diamonds). The maps geographic coordinate system refers to WGS84 UTM Zone 31N and is displayed in Mercator Projection.

2.2.4 Extrapolation of drilling-induced CH$_4$ leakage to the North Sea scale. CH$_4$ leakage from wells into the North Sea and atmosphere was calculated by extrapolating data obtained in the CNS (leakage rates, initial bubble size distributions, and the likelihood of wells to leak) and results of a numerical bubble dissolution model (SI Section 2.2.2) on the EMODnet North Sea bathymetry and combining publicly available data on drilled wells (SI Section 2.2.3) using the geographical information system software ArcGIS v10.1.

In total, 11 122 active and inactive wells were selected for the North Sea-wide CH$_4$ release quantification excluding sidetracks of wells (Table S4). The North Sea was subdivided into equal area polygons of 5×5 km^2 using a Cylindric Equal Area projection and the "Fishnet" tool of ArcGIS v.10.1. Spatial joining of the selected wells and bathymetric data gives each polygon a summary of numeric attributes that fall inside it, i.e. the average water depth (z) and a count field showing how many points fall inside it, i.e. the number of wells.

The seabed CH$_4$ flow (Q$_{SF}$) was calculated for each of these polygons multiplying the leakage probability (LP) of 33 ± 6% for the wells (SI Section 2.2.1), the number of wells located inside each polygon (AF, activity factor), and the potential range of per-well CH$_4$ leakage rates (LR) of 1-4 t yr^{-1}:

$$Q_{SF} = AF \times LP \times LR \qquad\qquad \text{Supplement Eq. (11)}$$

For each polygon, the resulting CH$_4$ flow from the surface water into the atmosphere (Q$_{Atm}$) was then estimated applying a transfer function describing the CH$_4$ bubble transport efficiency to the sea surface and to the SML of the North Sea (SI Section 2.2.2, Eq. S9 and S10) as a function of the seabed CH$_4$ flow (Q$_{SF}$) and average water depth of the polygon (z):

$$Q_{Atm,i} = Q_{SF,i} \times \Omega_{SML,i/S,i}(\psi.z) \qquad\qquad \text{Supplement Eq. (12)}$$

, where i is the leakage range (considering either the lower or upper range of possible leakage rates), and ψ is the common bubble size distribution (SI Section 2.1.3). Applying Supplementary Eq. 12, we assume no variation of initial bubble sizes over the extended area of the North Sea (SI Section 2.1.3) and that essentially all of the CH$_4$ reaching the SML will be transferred into the atmosphere.

All determined flow estimates of individual polygons, were added to calculate the potential range of the total CH_4 ebullition from the seafloor and into the atmosphere. Reported values of CH_4 leakage into the North Sea and the atmosphere are expressed in kilo tonnes of CH_4 per year (kt yr^{-1} of CH_4), considering the potential range of per-well leakage rates of 1-4 t yr^{-1} of CH_4 (N = 2)[20] and an uncertainty in the leakage frequency of 6% for the wells (N = 55).

2.2.5 Leakage from oil and gas infrastructure in a North Sea CH_4 context. We recalculated the CH_4 budget of the North Sea compiling quantitative literature data on major sources and sinks for marine CH_4 and adding the so-far unrecognized release of shallow gas along leaky wells quantified in this study (for results see Figure 3 and Table S5).

Existing estimates on North Sea-wide CH_4 emissions into the atmosphere are based on the extrapolation of point measurements of CH_4 concentrations in the near-surface seawater and the atmosphere[27, 30, 36]. The reported diffusive emissions into the atmosphere range from 10-50 kt yr^{-1} and are believed to already include the diffusive contribution of leaky wells (1-5 kt yr^{-1}), because their CH_4 anomalies are distributed over a broad area of the North Sea (Figure 4) and have thus, likely been detected during the measurement campaigns. In contrast, the blowout well 22/4b constitutes a very local, high flow CH_4 source in the British Sector. It was created in 1990, when Exxon Mobile accidently drilled into an over-pressurized shallow gas pocket. Its contribution to the atmospheric CH_4 flow was detected in only one[30] of the three surveys[27,30,36], 3.5 years after the incident occurred. According to the data of Rehder et al.[30], well 22/4b contributed 7-12 kt yr^{-1} to the total atmospheric flux of 50 kt yr^{-1} [30]. More recent studies suggest that the blowout well releases 2-25 kt yr^{-1} of CH_4 from the seabed[41-42], without transporting gas directly into the atmosphere[71]. The lack of direct bubble transport suggests that essentially all of the CH_4 released from the seabed dissolves in the water column where it is partly (~1-3%) oxidized by microbes[40]. The remaining CH_4 pool may reach the atmosphere by diffusive outgassing or may be exported to the Atlantic. In summertime, when the water column is stratified, most (~97%) of the CH_4 released at well 22/4b was found to not immediately reach the atmosphere, because it is trapped in the deep layer below the thermocline[41]. However, newly released CH_4 and the trapped, non-oxidized CH_4 pool are believed to be transported rapidly to the sea surface and emitted into the atmosphere in wintertime when the water column becomes well mixed as well as during storm events[41]. Current annual atmospheric emissions of well 22/4b are thus, believed to be similar to

those quantified by Rehder et al.[30] in their earlier conservative study. To incorporate our new data of drilling-induced CH_4 leakage, we recalculated the budget. Total emissions from the North Sea into the atmosphere comprise the range of existing quantifications on the diffusive gas exchange (10-50 kt yr^{-1} of CH_4) and direct bubble ebullition from leaky wells (0-2 kt yr^{-1} of CH_4) (Table S5).

The high super-saturation of the North Sea surface waters and the resulting atmospheric degassing of CH_4 constitute the major sink in the marine CH_4 budget (Table S5). Measured CH_4 oxidation rates in the water column were very low (Table 1), such that the microbial sink for CH_4 is expected to be negligible (Table S5). Adding direct bubble ebullition from leaky wells (0-2 kt yr^{-1} of CH_4) and the amount of CH_4, which is exported to the North Atlantic Ocean (8 kt yr^{-1})[30], the sinks for CH_4 are almost 20-times larger than the known natural sources (rivers, the Waddden Sea, and natural seeps). The North Sea-wide CH_4 input from drilling-induced leakage (leaky wells and blowout well 22/4b), thus likely contributes significantly to the CH_4 budget (see Figure 3 and Table S5). It should be noted that our estimate of CH_4 seepage from natural seeps is based on the few available quantitative measurements that are currently available (Table S5). The numerous natural gas seeps with unknown emission rates that are present in the North Sea may add more CH_4 and contribute significantly to the overall CH_4 input[23].

Table S5 |Sources and sinks for CH_4 in the North Sea. Bold values have been taken to recalculate the CH_4 budget of the North Sea.

CH_4 Sources	Input/ t yr^{-1} of CH_4	Reference
Natural seeps		
Scanner Pockmark Field*	0.1-13	Judd and Hovland [31] and references therein; Hovland et al. [34] and references therein
UK Block 15/25	7±?	Judd [33] and references therein
Anvil Point UK	68±?	Judd [33] and references therein

Torre Bay Firth of Fourth	1-2	Judd [33] and references therein
Tommeliten	26-42	Schneider von Deimling et al.[32] (lower bound); Judd [33] (upper bound)
Norwegian Block 1/9 Ekosfisk**	52±?	Judd and Hovland [31] and references therein; Hovland et al. [34] and references therein
Total input via seeps	**>0.2×10³**	
Rivers		
Rhine	339	Upstill-Goddard et al. [27]
Weser	86	Grunwald et al. [28]
Wash	61	Upstill-Goddard et al. [27]
Elbe	35	Rehder et al. [30]; Grunwald et al. [28] and references therein
Humber	5	Upstill-Goddard et al. [27]
Tyne	2	Upstill-Goddard et al. [27]
Sheldt	22-34	Scranton and McShane [29]
Total riverine input	**0.6±? ×10³**	
Wadden Sea		
Spiekeroog Island back barrier area	53	Grunwald et al. [28]
East Frisian back barrier area	125	Grunwald et al. [28]
Entire back barrier tidal flats*	**1.0-2.1 ×10³**	Based on Grunwald et al. [28] and references therein
Hydrocarbon infrastructure		
Blowout well 22/4b	2-25 ×10³	Sommer et al. [41] (lower bound); Leifer[42] (upper bound)

	Loss/ t yr^{-1} of CH$_4$	Reference
Shallow gas migration	3-17 $\times 10^3$	This study
Total HC infrastructure	**5-43 $\times 10^3$**	

CH$_4$ sinks	**Loss/ t yr^{-1} of CH$_4$**	**Reference**
Atmosphere		
Diffusive gas exchange (excl. 22/4b)	10-34 $\times 10^3$	Bange et al. [36] and Upstill-Goddard et al. [27] (lower bound); Rehder et al. [30] (upper bound)
Diffusive gas exchange (incl. 22/4b)	30-50 $\times 10^3$	Rehder et al. [30]
Diffusive contribution from shallow gas migration along wells	1-5 $\times 10^3$	This study (Range considering a per-well leakage rates of 1-4 t yr^{-1} of CH$_4$ and an uncertainty in the leakage frequency of 6%)
Direct ebullition from shallow gas migration along wells	0-2 $\times 10^3$	This study (Range considering a per-well leakage rates of 1-4 t yr^{-1} of CH$_4$ and an uncertainty in the leakage frequency of 6%)
Total losses into the atmosphere	**10-52 $\times 10^3$**	This study (diffusive gas exchange and direct ebullition)
Microbial CH$_4$ oxidation at leaky wells****	**0.02 $\times 10^3$±?**	This study
Microbial CH$_4$ oxidation at blowout well 22/4b	**0.02-0.8$\times 10^3$**	Steinle et al. [40] (considering that 1-3% of recent oceanic emissions of well 22/4b are oxidized)
CH$_4$ export to North Atlantic Ocean	**8 $\times 10^3$**	Rehder et al. [30]

Total CH$_4$ Budget	Total CH$_4$ sources	Total CH$_4$ sinks
kt yr^{-1} of CH$_4$	7-46	18-60

Assuming a gas flow of 5.7 L h^{-1} $seep^{-1}$ at STP [31] and 3 active seeps [34], the Scanner Pockmark field emits 0.1 t yr^{-1} of CH_4 (lower bound). Assuming a seabed gas flow of 1 m^3 d^{-1} $seep^{-1}$ [34], a molar volume of CH_4 of 1.34 L mol^{-1} at 160 m water depth, and 3 active seeps [34], the Scanner Pockmark field emits ~13 t yr^{-1} of CH_4 (upper bound).

*** Based on a seabed emission of ~24 m^3 d^{-1} of CH_4 [31, 34] and assuming a molar volume of CH_4 of 2.69 L mol^{-1} at 75 water depth, the Norwegian Block 1/9 emits ~52 t yr^{-1} of CH_4.*

**** We extrapolated the CH_4 export of the East Frisian back barrier area (125 t yr^{-1} of CH_4 per 197 km^2 [28] on the entire back barrier tidal flat area from Den Helder to Esbjerg (1188-3364 km^2)[28] assuming that the CH_4 concentrations and the water outflow of the Spiekeroog study area[28] are representative.*

***** We estimated the loss of CH_4 by methanotrohic communities at leaky wells, based on the maximum measured CH_4 oxidation rate of 1.4 nM d^{-1}(this study), a leakage area of 10 m^2 $well^{-1}$ [20], and an average leakage depth of 80 m (in accordance to the spatial distribution of wells and the North Sea bathymetry).*

2.2.6 Sources of uncertainty in our estimates. The range of uncertainty of shallow gas leakage in the North Sea is substantial, as might be expected from the current state of knowledge of leaky wells, mainly depending on the representativeness of data obtained in the Norwegian CNS. There is a large uncertainty in our estimates related to the unknown temporal and spatial variability of per-well leakage rates that might, in addition to sediment properties and tidal pressure fluctuations, be driven by overpressure in the shallow gas reservoir, or by differences in the gas supply. Further uncertainty is associated to the probability of wells to leak shallow gas. Assuming a binomial distribution from a Bernoulli process, the uncertainty in the frequency of leakage that a sample size of 55 wells would produce in the larger population of wells is believed to be small (i.e. ± 6% 1-σ) compared to the uncertainty in the leakage rate per well. Our estimate for CH_4 leakage from hydrocarbon wells in the North Sea is based on the two lower leakage rates and the assumption that wells poking through shallow gas pockets will leak, which is corroborated by observed ebullition of biogenic gas at wells 15/9-13 and 16/7-2[20] as well as 15/9-11 and 15/9-16[43]. Surveying for leaky wells and quantifying their ebullition rates (including longer time-series) is clearly needed in order to better constrain the North Sea CH_4 budget.

Atmospheric emission estimates bear further uncertainty arising from three additional factors: (1) temporal and spatial variability of the bubble chain dynamics (upwelling), (2) variability of initial

bubble sizes, and (3) seasonal/ inter-annual changes of seawater conditions. The latter may significantly affect the diffusive outgassing of CH_4 due to the seasonal deepening and breakdown of the thermocline[30, 32,37,41] and the efficient ventilation of the entire water column during frequent fall and winter storms, which both should aid annual diffusive CH_4 emissions. No significant inter-annual variability is expected in the rate of direct CH_4 ebullition to the atmosphere because the bubble CH_4 transport is independent of the water column stratification and also nearly temperature-independent. This is because the increase in gas transfer velocity (K_L) compensates the decrease in gas solubility at elevated temperature. The approach to estimate atmospheric emissions is thus, believed to be conservative because the gas transport to the atmosphere might has been underestimated due to the seasonal increase in the ventilation of the water column or the evidence of upwelling flows at high-emitting seeps. Uncertainties related to initial bubble sizes remain, which might, in addition to spatial heterogeneities in the sediment properties, be driven by variations in the seabed gas flow, or bottom current intensity, or changes in the hydrostatic pressure[38].

2.2.7 Generality of our approach for assessing CH_4 emissions along wells in other regions that have undergone extensive offshore drilling. Shallow gas migration along hydrocarbon wells has not received much attention yet and data on leakage rates are limited to those observed at the three abandoned gas wells in the North Sea[20]. Given the small sample size and unknown temporal and spatial variability of per-well leakage rates, the uncertainties behind annual, regional flux estimates are generally large (as discussed above). Due to regional differences in geology, the leakage rates (1-19 t yr^{-1} of CH_4 per well)[20] and leakage frequency of wells (33 ± 6%) observed in the North Sea might not be appropriate for extrapolation to other regions that are rich in shallow gas and have undergone extensive offshore drilling. More measurements (including longer time series) are clearly needed to better constrain leakage rates and leakage pathways (i.e. gas migration along the well vs. well annulus leakage), both onshore and offshore.

Our numerical results to estimate atmospheric CH_4 emissions from submarine gas leaks indicate that wells (and seeps) located in water depths larger than 150 m generally do not contribute significant CH_4 to the atmosphere (see Figure S5, justified for initial bubble radii up to 4 mm), but rather contribute to CH_4 in the deep-water layer where it is transported by ocean currents and prone to microbial oxidation. Some unknown fraction of this deeply dissolved CH_4 may be mixed

into the surface mixed layer during storms and seasonal or inter-annual deepening and breakdown of the thermocline. The gas bubble dissolution rate is rather temperature-independent (see SI Section 2.2.6), suggesting that our numerical results (i.e. Supplementary Eq. 6, 9 and 10) are applicable for assessing approximate atmospheric CH_4 contributions in a variety of coastal (≤ 150 m water depth) marine and lacustrine regions (e.g. from the Gulf of Mexico to the Arctic). Supplementary Eq. 6 describes the transport efficiency of CH_4 bubbles to the sea surface with respect to the seabed CH_4 flow and as a function of the initial bubble size (justified for initial radii of 1-4 mm) and the leakage depth. Supplementary Eq. 9 and 10 describe the transport efficiency of CH_4 bubbles with a specific bubble size distribution (i.e. $r_e=2.6$ mm[20], SI Figure S5) to the sea surface (Eq. S9) and to the SML (Eq. S10) with respect to the seabed CH_4 flow and as a function of the leakage depth, respectively. Their application is generally justified in marine regions up to 150 m water depth, where clean CH_4 bubbles, that initially contain only CH_4, rise in the absence of bubble plume dynamics (i.e. by the release of single bubble streams that do not induce upwelling). The general applicability of Eq. S10 to estimate the diffusive outgassing of CH_4 is limited due to regional differences in water column stratification and mixing (i.e. Eq. S10 considers the diffusive outgassing of CH_4 dissolved in the upper 50 m of the water column).

Our transfer functions (Eq. S6, S9, S10) are not suitable for assessing atmospheric CH_4 emissions in regions where gas bubbles are coated with oil, hydrates, and/or other surfactants, which generally prevent the gas exchange with ambient seawater and thus, favor the bubble-driven transport of seabed CH_4 to the surface. Further limitations are related to bubble plumes that generate upwelling, turbulences[71], and/or spiral movement[72], which affect the rate of bubble dissolution and have not been considered in our numerical simulations.

SI References

(1) Ciais, P., et al. Carbon and other biogeochemical cycles. In *Climate Change 2013: The Physical Science Basis. Contribution of Working Group I to the Fifth Assessment Report of the Intergovernmental Panel on Climate Change*; Stocker, T. F., Qin, D., Plattner, G.-K., Tignor, M., Allen, S. K., Boschung, J., Nauels, A., Xia, Y., Bex, V., Midgley, P. M., Eds.; IPCC: Cambridge, UK, 2013; pp 465−570.
(2) Davies, R. J.; et al. Oil and gas wells and their integrity: Implications for shale and unconventional resource exploitation. *Mar. Pet. Geol.* **2014**, *56*, 239−154. 392
(3) *Well integrity in drilling and well operations, NORSOK Standard D-010,* 2004. http://www.standard.no/PageFiles/1315/D-010r3.pdf.

(4) Allen, D. T.; et al. Measurements of methane emissions at natural gas production sites in the United States. *Proc. Natl. Acad. Sci. U. S. A.* **2013**, *110*, 17 768−17 773.

(5) Alvarez, R. A.; Pacala, S. W.; Winebrake, J. J.; Chameides, W. L.; Hamburg, S. P. Greater focus needed on methane leakage from natural gas infrastructure. *Proc. Natl. Acad. Sci. U. S. A.* **2012**, *109*, 6435−6440.

(6) Caulton, D. R.; et al. Toward a better understanding and quantification of methane emissions from shale gas development. *Proc. Natl. Acad. Sci. U. S. A.* **2014**, *111*, 6237−6242.

(7) Miller, S. M.; et al. Anthropogenic emissions of methane in the United States. *Proc. Natl. Acad. Sci. U. S. A.* **2013**, *110*, 20 018−20 022.

(8) Schneising, O.; et al. Remote sensing of fugitive methane emissions from oil and gas production in North American tight geologic formations. *Earth's Future* **2014**, *2*, 548−558.

(9) Zhang, Y.; Zhao, H.; Zhai, W.; Zang, K.; Wang, J. Enhanced methane emissions from oil and gas exploration areas to the atmosphere − The central Bohai Sea. *Mar. Pollut. Bull.* **2014**, *81*, 157−165.

(10) Brandt.; et al. Methane Leaks from North American Natural Gas Systems. *Science* **2014**, *343*, 733−735.

(11) Balcombe, P.; Anderson, K.; Speirs, J.; Brandon, N.; Hawkes, A. The Natural Gas Supply Chain: The Importance of Methane and Carbon Dioxide Emissions. *ACS Sustainable Chem. Eng.* **2017**, *5*, 3−20.

(12) Kang, M.; et al. Direct measurements of methane emissions from abandoned oil and gas wells in Pennsylvania. *Proc. Natl. Acad. Sci. U. S. A.* **2014**, *111*, 18 173−18 177.

(13) Kang, M.; et al. Identification and characterization of high methane-emitting abandoned oil and gas wells. *Proc. Natl. Acad. Sci. U.S. A.* **2016**, *113*, 13 636−13 641.

(14) Townsend-Small, A.; Ferrara, T. W.; Lyon, D. R.; Fries, A. E.; Lamb, B. K. Emissions of coalbed and natural gas methane from abandoned oil and gas wells in the United States. *Geophys. Res. Lett.* **2016**, *43*, 2283−2290.

(15) Boothroyd, I. M.; Almond, L.; Qassim, S. M.; Worrall, F.; Davies, R. J. Fugitive emissions of methane from abandoned, decommissioned oil and gas wells. *Sci. Total Environ.* **2016**, *547*, 461−469.

(16) Brufatto, C.; et al. From mud to cement - Building gas wells. *Oilfield Rev.* **2003**, *15*, 62−76.

(17) Alberta Energy and Utilities Board. *Interim Directive ID 2003-01*; 2003.

(18) Watson, T. L.; Bachu, S. Evaluation of the potential for gas and CO_2 leakage along wellbores. *SPE Drill. Compl.* **2009**, *24*, 115−26.

(19) Erno, B.; Schmitz, R. Measurements of soil gas migration around oil and gas wells in the Lloydminster area. *J. Can. Pet. Technol.* **1996**, *35*, 37−45.

(20) Vielstädte, L.; et al. Quantification of methane emissions at abandoned gas wells in the Central North Sea. *Mar. Pet. Geol.* **2015**, *68*, 848−860.

(21) Gurevich, A. E.; Endres, B. L.; Robertson, J. O.; Chilingar, G. V. Gas migration from oil and gas fields and associated hazards. *J. Pet. Sci. Eng.* **1993**, *9*, 223−238.

(22) Løseth, H.; Gading, M.; Wensaas, L. Hydrocarbon leakage interpreted on seismic data. *Mar. Pet. Geol.* **2009**, *26*, 1304−1319.

(23) Judd, A.; et al. Contributions to atmospheric methane by natural seepage on the U.K. *Mar. Geol.* **1997**, *140*, 427−455.

(24) Karstens, J.; Berndt, C. Seismic chimneys in the Southern Viking Graben- Implications for paleo fluid migration and overpressure evolution. *Earth Planet. Sci. Lett.* **2015**, *412*, 88−100.

(25) Schroot, B. M.; Klaver, G. T.; Schüttenhelm, R. T. E. Surface and subsurface expressions of gas seepage to the seabed- examples from the Southern North Sea. *Mar. Pet. Geol.* **2005**, *22*, 499−515.

(26) Schlüter, M., Jerosch, K. *Digital Atlas of the North Sea, version 0.9*; Alfred Wegener Institute for Polar and Marine Research et al., 2009; hdl:10012/epic.34893.d001.

(27) Upstill-Goddard, R. C.; Barnes, J.; Frost, T.; Punshon, S.; Owens, N. J. P. Methane in the southern North Sea: Low-salinity inputs, estuarine removal, and atmospheric flux. Glob. *Biogeochem. Cycles* **2000**, *14* (4), 1205−1217.

(28) Grunwald, M.; et al. Methane in the southern North Sea, spatial distribution and budgets. Estuarine, *Coastal Shelf Sci.* **2009**, *81*, 445− 456.

(29) Scranton, M. I.; McShane, K. Methane fluxes in the southern North-Sea − the role of European rivers. *Cont. Shelf Res.* **1991**, *11*, 37− 52.

(30) Rehder, G.; Keir, R. S.; Suess, E.; Pohlmann, T. The multiple sources and patterns of methane in North Sea waters. *Aquat. Geochem.* **1998**, *4*, 403−427.

(31) Judd, A. G., Hovland, M. *Seabed Fluid Flow: The Impact on Geology, Biology and Marine Environment*; Cambridge University Press: New York, 2007.

(32) Schneider von Deimling, J.; et al. Quantification of seep-related methane gas emissions at Tommeliten, North Sea. *Cont. Shelf Res.* **2011**, *31*, 867−878. 478

(33) Judd, A. G. Natural seabed gas seeps as sources of atmospheric methane. *Environ. Geol.* **2004**, *46*, 988−996.

(34) Hovland, M.; Jensen, S.; Fichler, C. Methane and minor oil macro-seep systems − Their complexity and environmental significance. *Mar. Geol.* **2012**, *332−334*, 163−173.

(35) Borges, A. V.; Champenois, W.; Gypens, N.; Delille, B.; Harlay, J. Massive marine methane emissions from near-shore shallow coastal area. *Sci. Rep.* **2016**, *6*, 27 908.

(36) Bange, H. W.; Bartell, U. H.; Rapsomanikis, S.; Andreae, M. O. Methane in the Baltic and North Seas and a reassessment of the marine emissions of methane. *Glob. Biogeochem. Cycles* **1994**, *8*, 465− 480.

(37) Thomas, H.; et al. The carbon budget of the North Sea. *Biogeosciences* **2005**, *2*, 87−96.

(38) Dewar, M.; Wei, W.; McNeil, D.; Chen, B. Small-scale modelling of the physicochemical impacts of CO_2 leaked from sub-seabed reservoirs or pipelines within the North Sea and surrounding waters. *Mar. Pollut. Bull.* **2013**, *73*, 504−515.

(39) Steinle, L.; et al. Water column methanotrophy controlled by a rapid oceanographic switch. *Nat. Geosci.* **2015**, *8*, 378−383.

(40) Steinle, L.; Schmidt, M.; Bryant, L; Haeckel, M.; Linke, P.; Sommer, S.; Zopfi, J.; Lehmann, M. F.; Treude, T.; Niemann, H. Linked sediment and water-column methanotrophy at a man-made gas blowout in the North Sea: Implications for methane budgeting in seasonally stratified shallow seas. *Limnol. Oceanogr.* **2016**, *61*, 367−386.

(41) Sommer, S.; Schmidt, M.; Linke, P. Continuous inline mapping of a dissolved methane plume at a blowout site in the Central North Sea UK using a membrane inlet mass spectrometer − water column stratification impedes immediate methane release into the atmosphere. *Mar. Pet. Geol.* **2015**, *68*, 766−775.

(42) Leifer, I. Seabed bubble flux estimation by calibrated video survey for a large blowout seep in the North Sea. *Mar. Pet. Geol.* **2015**, *68*, 743−752.

(43) Pedersen, R. B.; et al. *ECO2 Deliverable 1.1: Report of Leakage Assessment;* 2013. http://dx.doi.org/10.3289/ECO2_D1.1.

(44) Thorpe, A. K.; et al. Mapping methane concentrations from a controlled release experiment using the next generation airborne visible/infrared imaging spectrometer (AVIRIS-NG). *Remote Sens. Environ.* **2016**, *179*, 104−115.

(45) *NPD Guidelines for Designation of Wells and Wellbores*, 2014. http://www.npd.no/Global/Norsk/5Regelverk/Tematiskeveiledninger/Bronner_betegnelser_og_kl assifisering_e.pdf

(46) Rehder, G.; Schneider von Deimling, J. RV *Sonne Cruise Report SO 196 SUMSUN. Leibniz Institute for Baltic Sea Research*, Warnemünde 2008, 77; DOI PANGAEA, hdl: 10013/epic.35734.

(47) Pape, T.; et al. Molecular and isotopic partitioning of low-molecular-weight hydrocarbons during migration and gas hydrate precipitation in deposits of a high-flux seepage site. *Chem. Geol.* **2010**, *269*, 350–363.

(48) Bernard, B. B.; Brooks, J. M.; Sackett, W. M. Light hydro-carbons in recent Texas continental shelf and slope sediments. *J. Geophy. Res.* **1987**, *83*, 4053-4061.

(49) James, A. T. Correlation of reservoired gases using the carbon isotopic compositions of wet gas Components. *Am. Assoc. Petr. Geol. B.* **1990**, *74*, 1441-1458.

(50) Judd, A. G.; Hovland, M. The evidence of shallow gas in marine sediments. *Cont. Shelf Res.* **1992**, *12*, 1081-1095.

(51) Farreira, T.; Rasband, W. *ImageJ User Guide IJ 1.46r*, 2012. http://imagej.nih.gov/ij/docs/guide/index.html

(52) Clift, R.; Grace, J. R.; Weber, M. E. *Bubbles, Drops, and Particles;* Academic Press: London, 1978.

(53) Linke, P.; Schmidt, M.; Rohleder, M.; Al-Barakati, A.; Al-Farawati, R. Novel online digital video and high-speed data broadcasting via standard coaxial cable onboard marine operating vessels. *Mar. Technol. Soc. J.* **2015**, *49* (1), 7-18.

(54) Blees, J.; et al. Micro-aerobic bacterial methane oxidation in the chemocline and anoxic water column of deep south-Alpine Lake Lugano (Switzerland). *Limnol. Oceanogr.* **2014**, *59* (2), 311–324.

(55) Treude, T.; Boetius, A.; Knittel, K.; Wallmann, K.; Jørgensen, B. B. Anaerobic oxidation of methane above gas hydrates at Hydrate Ridge, NE Pacific Ocean. *Mar. Ecol. Prog. Ser.* **2003**, *264*, 1–14.

(56) de Anglis, M. A.; Lilley, M. D.; Olson, E. J.; Baross, J. A. Methane oxidation in deep-sea hydrothermal plumes of the Endeavor Segment of the Juan de Fuca Ridge. *Deep Sea Res. 1* **1993**, *8*, 1169-1189.

(57) Mau, S.; Heintz, M. B.; Valentine, D. L. Quantification of CH_4 loss and transport in dissolved plumes of the Santa Barbara Channel, California. *Cont. Shelf Res.* **2012**, *32*, 110-120.

(58) Heeschen, K. U.; et al. Methane sources, distributions, and fluxes from cold vent sites at Hydrate Ridge, Cascadia Margin. *Glob. Biogeoche. Cycles* **2005**, *19*: GB2016.

(59) Crespo-Medina, M.; et al. The rise and fall of methanotrophy following a deepwater oil-well blowout. *Nature Geosci.* **2014**, *7*, 423-427.

(60) Duan, Z. H.; Moller N.; Weare, J. H. An equation of state for the CH_4-CO_2-H_2O system: I. Pure systems from 0-1000°C and from 0 to 8000 bar. *Geochim. Cosmochim. Acta* **1992**, *56*, 2605-2617.

(61) Duan, Z. H.; Mao, S. A hermodynamic model for calculating methane solubility, density and gas phase composition of methane-bearing aqueous fluids from 273 to 523 K and from 1 to 2000 bar. *Geochim. Cosmochim. Acta* **2006**, *7*, 3369-3386.

(62) Geng, M.; Duan, Z. H. Prediction of oxygen solubility in pure water and brines up to high temperatures and pressures. *Geochim. Cosmochim. Acta* **2010**, *74*, 5631-5640.

(63) Mao, S.; Duan, Z. H. A thermodynamic model for calculating nitrogen solubility, gas phase composition and density of the N_2-H_2O-NaCl-system. *Fluid Phase Equilibr.* **2006**, *248*, 103-114.

(64) Boudreau, B. P. *Diagenetic Models and their Implementation: Modelling Transport and Reactions in Aquatic Sediments*; Berlin, Heidelberg, New York, London, Paris, Tokyo, Hong Kong: Springer, 414 pp, 1997.

(65) Zheng, L.,; Yapa, P. D. Modeling gas dissolution in deepwater oil/gas spills. *J. Marine Syst.* **2002**, *31*, 299-309.

(66) Wüest, A.; Brooks, N. H.; Imboden, D. N. Bubble plume modeling for lake restoration, *Water Resour. Res.* **1992**, *28* (12), 3235–3250.

(67) Sofroniou, M.; Knapp, R. *Wolfram Mathematica Tutorial Collection- Advanced numerical differential equation solving in Mathematica. Wolfram Research Inc*, 2008. http://www.wolfram.com/learningcenter/tutorialcollection/AdvancedNumericalDifferentialEquati onSolvingInMathematica/AdvancedNumericalDifferentialEquationSolvingInMathematica.pdf

(68) McGinnis, D. F.; Little J. C. Predicting diffused-bubble oxygen transfer rate using the discrete-bubble model. *Water Res.* **2002**, *36*, 4627–4635.

(69) Leifer, I.; Patro, R. K. The bubble mechanism for methane transport from the shallow sea bed to the surface: A review and sensitivity study. *Cont. Shelf Res.* **2002**, *22*, 2409–2428.

(70) UNESCO. The Practical Salinity Scale 1978 and the International Equation of State of Seawater 1980. *Tech. Pap. Mar. Sci.* **1981**, *36*, 25 pp.

(71) Leifer, I.; et al. The fate of bubbles in a large, intense bubble megaplume for stratified and unstratified water: Numerical simulation of 22/4b Expedition field data. *Mar. Petrol. Geol.* **2015**, *68*, 806-823.

(72) Schneider von Deimling, J.; Linke, P.; Schmidt, M.; Rehder, G. Ongoing methane discharge at well site 22/4b (North Sea) and discovery of a spiral vortex bubble plume motion. *Mar. Petrol. Geol.* **2015**, *68*, 718-730.